The 2010 IEEE/RSJ International Conference on
Intelligent Robots and Systems
October 18-22, 2010, Taipei, Taiwan

Optimal Design and Fabrication of a Piezoactuated Flexure XYZ Parallel Micropositioning Stage

Qingsong Xu, *Member, IEEE*, and Yangmin Li, *Senior Member, IEEE*

***Abstract*— This paper presents the design and fabrication process of a new piezoelectrically actuated flexure-based XYZ compliant parallel-kinematics micropositioning stage with totally decoupled properties. The proposed XYZ stage consists of three limbs which are assembled in an orthogonal manner, and it has both input and output decoupling properties. Analytical models for kinematics, statics, and dynamics of the XYZ stage are established, which are validated by finite element analysis performed with ANSYS. Based on the derived models, architectural parameters of the stage are optimized and a prototype is developed for experimental studies. The results not only verify the effectiveness of the conducted optimum design but also confirm the well-decoupled performance of the XYZ stage, which will be used to execute micro-/nanomanipulation tasks.**

I. INTRODUCTION

Flexure-based micropositioning stages are the devices capable of positioning with ultrahigh precision based on the elastic deformations of the material [1]–[5]. They can be found in a variety of applications involving optical fiber alignment, biological cell manipulation, and scanning probe microscopy (SPM), etc. In view of the high-resolution motion requirement of the said applications, the stages are usually driven by unconventional motors, such as piezoelectric actuators (PZTs), voice coil motors, magnetic levitation motors, and so on.

In particular, XYZ positioning stage is an ideal choice for many situations where a 3-D translation is sufficient, e.g., the scanning device in an atomic force microscope (AFM). Some compliant XYZ stages are even commercially available on the market. For instance, the XYZ stage [6] produced by the PI adopts a stacked structure of three one-DOF (degree of freedom) positioning stages. The serial connection of three stages enables a simple control strategy since the X, Y, and Z translations can be governed independently, which is at the cost of a relatively low resonant frequency of the mechanism since the stacked stage increases the mass of moving components. It is known that in the AFM, a high-speed positioning of the stage is required to implement a rapid scanning task. Thus, high resonant frequency is preferred for the mechanism design of the positioning stage.

To conquer the above shortcomings of serial stages, XYZ stages with parallel-kinematics architectures [7] have gained extensive attentions. A number of XYZ stages with parallel kinematics have been reported in the literature [8]–[11]. However, most of the existing XYZ stages have a coupled motion. In some situations where the sensory feedback for the displacements of stage output platform can not be realized, a decoupled XYZ stage with proper calibrations is preferred [3]. Moreover, a decoupled stage will also benefit the controller design process, since single-input-single-output (SISO) control schemes are sufficient. Generally, a decoupled stage implies that one motor produces only one directional output motion while does not affect the motion in other axes. The term of "decoupled" refers to the output motion decoupling of the stage. Nevertheless, the input decoupling [12] is rarely regarded since it emphasizes on the isolation of the input motion instead. When the stage is driven by one motor, other motors may suffer from unwanted loads due to the movement of the output platform, or clearances between other motors and the interfacing points with the stage may occur. Even though the clearance problem can be solved by using preloaded springs, the presence of unwanted transverse loads may damage some types of motors such as PZT. To cope with such difficulties, a concept of totally decoupling is presented in recent works [13] of the authors to design a compliant-based XY positioning stage with both input and output decoupling merits.

In this research, the design of an XYZ totally decoupled parallel stage (TDPS) is outlined. Among previous works on XYZ compliant parallel stages, the one presented in [14] can be classified into this category. Such an XYZ stage consists of a total of nine individual prismatic (P) hinges, which are assembled together to construct a 3-PPP parallel mechanism. Intuitively, the excessive assembly of the complex joints may degrade the accuracy property of the stage. Additionally, the presented stage is directly driven by linear motors, which results in a stage workspace equal to the travel stroke of the motors. In case that the stroke is not satisfied, a displacement amplification device is desirable. However, additional displacement amplifiers for this stage will complicate its structure even more. So, the predominant goal of the current research is to design an XYZ TDPS with a displacement amplifier and an architecture as simple as possible for the ease of manufacture.

Once the structure of the stage is designed, it is necessary to determine its architectural parameters in order to achieve better performances. For such a purpose, the establishment of analytical models for performance predications of the stage is necessary. In the rest of the paper, the design process of the new XYZ stage is presented in Section II.

This work was supported by Macao Science and Technology Development Fund under Grant 016/2008/A1 and the research committee of University of Macau under Grant UL016/08-Y2/EME/LYM01/FST.

The authors are with the Department of Electromechanical Engineering, Faculty of Science and Technology, University of Macau, Av. Padre Tomás Pereira, Taipa, Macao SAR, P. R. China. Corresponding author Y. Li: ymli@umac.mo

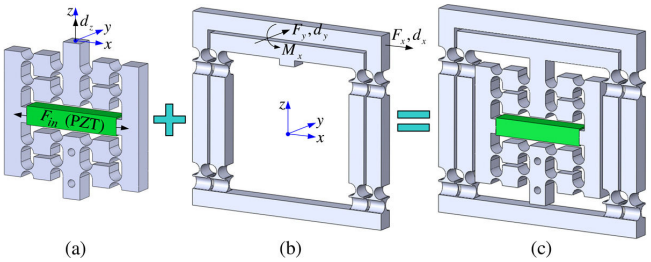

Fig. 1. (a) A compound bridge-type displacement amplifier with certain tolerance of lateral load; (b) a 2-DOF linear guiding mechanism using a compound parallelogram flexure; (c) a monolithic PPP limb with decoupled translations.

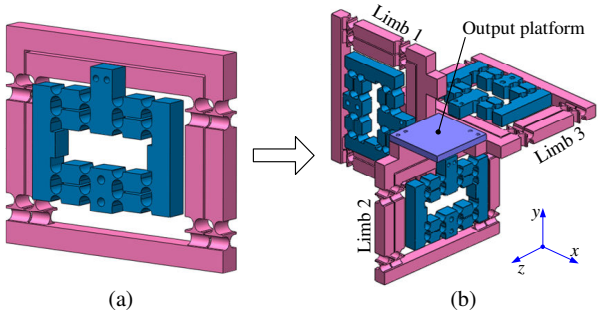

Fig. 2. (a) A two-layered PPP limb with decoupled translations; (b) a decoupled XYZ stage composed of three limbs.

Then, mechanical modeling is carried out and validated with FEA in Sections III and IV, respectively. Afterwards, the dimension optimization of the stage is realized in Section V, and a prototype is fabricated for performance tests in Section VI. Finally, Section VII concludes this paper.

II. MECHANISM DESCRIPTION OF THE XYZ STAGE

The primary objective for the design of an XYZ stage with decoupled output motion is to eliminate the cross-axis coupling errors between the X, Y, and Z directional translations and the parasitic rotation errors around the axes. On the other hand, since the stage will be driven by three linear motors, it is important to make sure that when one motor drives the stage to move along the pertinent axis, the motor bears neither transverse loads nor transverse displacements induced by the other two motors driving the stage along the remaining two axes.

Specifically, the compound bridge-type displacement amplifier [see Fig. 1(a)] can provide both an amplified linear guiding output motion in the vertical direction (z-axis) and a spring preload for the linear actuator. Besides, this type of amplifier has much larger input stiffness and larger lateral stiffness than the conventional bridge-type amplifier. The large input stiffness calls for an actuator with large blocking force and stiffness. Hence, PZT is the most suitable actuator for the drives of the amplifier. On the other hand, the large lateral stiffness indicates that the output end of the amplifier can tolerate a large lateral load. This merit provides protection for the inner PZT which can only tolerate small magnitude of lateral load.

In addition, by orthogonally adding a pair of flexure hinges to each leg of the conventional 1-D compound parallelogram flexure translational stage, a 2-D spatial stage is constructed as shown in Fig. 1(b). By imposing an external force F_x, the output stage displays a pure translation along the x-axis due to the same length for the four R-R legs. Besides, by applying a force F_y and a moment M_x to the output stage, the stage will produce a pure translation along the y-axis, while without cross-axis errors in neither x-axis nor z-axis direction. It is noticeable that in an XYZ stage constructed later, the additional moment M_x for one limb mentioned above is produced by the other two limbs constructing the overall stage.

Thus, by combining the preceding amplifier with the 2-DOF linear guiding mechanism, a monolithic 3-D PPP limb with decoupled translations is obtained as shown in Fig. 1(c). Furthermore, for the ease of fabrications using such processes as wire electrical discharge machining (EDM), the amplifier is attached to the PP limb in a two-layered manner as depicted in Fig. 2(a). This PPP limb can be employed as a basic component to design an XYZ parallel stage with decoupled structure. For example, employing three such limbs, a totally decoupled XYZ stage is constructed as shown in Fig. 2(b), where the idea of orthogonal arrangement [14], [15] is adopted to assemble the three limbs together. In addition, the three limbs are assembled in such a way that the actuation axes of the limbs intersect at one common point. This assembly scheme is utilized to eliminate the unwanted internal moments which will occur if the actuation axes do not intersect at one common point. Both the input decoupling and output decoupling properties are expected from the XYZ stage, and the stage performances are assessed in the following discussions by establishing analytical models first.

III. SYSTEM MODELING

This section derives simple analytical models of the stage for the evaluation of its amplification ratio, input stiffness, stress, and natural frequency, which can be used for the performance assessment and cost-effective optimum design of the stage.

A. Kinematics and Statics Modeling

Due to a decoupled and parallel kinematics structure, the properties in the three working axes of the XYZ stage are identical in theory. Given the input displacements (d_1, d_2, and d_3) of the three PZT actuators, the stage output motion (d_x, d_y, and d_z) and the actuator input forces (F_1, F_2, and F_3) can be calculated by the following kinematics and statics equations:

$$\begin{bmatrix} d_x \\ d_y \\ d_z \end{bmatrix} = \begin{bmatrix} A_s & 0 & 0 \\ 0 & A_s & 0 \\ 0 & 0 & A_s \end{bmatrix} \begin{bmatrix} d_1 \\ d_2 \\ d_3 \end{bmatrix}, \tag{1}$$

$$\begin{bmatrix} F_1 \\ F_2 \\ F_3 \end{bmatrix} = \begin{bmatrix} K_a & 0 & 0 \\ 0 & K_a & 0 \\ 0 & 0 & K_a \end{bmatrix} \begin{bmatrix} d_1 \\ d_2 \\ d_3 \end{bmatrix}, \tag{2}$$

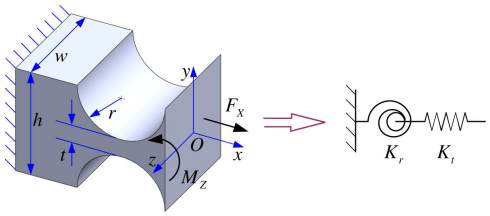

Fig. 3. A right-circular flexure hinge and its simplified model.

where A_s is the amplification ratio of the displacement amplifier, and K_a is the input (or actuation) stiffness of the stage, respectively.

Based on above relations, the kinematics and statics problems are converted to the calculation of amplification ratio and input stiffness of the XYZ stage, respectively. By simplifying each hinge as a joint with 2-DOF compliances (C_r and C_t), the joint can be represented by a torsional spring and a linear spring (see Fig. 3) with the stiffnesses of K_r and K_t, respectively. After a necessary static force analysis, the stage amplification ratio and input stiffness can be derived as:

$$A_s = \frac{l_a^2 l_8^2 K_t^2 \cos^3\alpha \sin\alpha}{(16K_r + l_8^2 K_t)(2K_r + l_a^2 K_B \cos^2\alpha + l_a^2 K_t \cos^2\alpha \sin^2\alpha)}, \tag{3}$$

$$K_a = \frac{2K_t \cos^2\alpha (2K_r + l_a^2 K_B \cos^2\alpha)}{2K_r + l_a^2 K_B \cos^2\alpha + l_a^2 K_t \cos^2\alpha \sin^2\alpha}, \tag{4}$$

where $l_a = \sqrt{l_1^2 + l_2^2}$, $\alpha = \text{atan}(l_2/l_1)$, and $K_B = 4K_rK_t/(16K_r + l_8^2 K_t)$. The detailed modeling procedure will be presented in another paper.

B. Workspace and Stress Analysis

With Q denoting the stroke of the adopted PZT, the workspace range of the XYZ stage can be derived as $A_sQ \times A_sQ \times A_sQ$ as long as the maximum stress due to the rotations (σ_r) and axial loads (σ_t) of flexure hinges remain within the allowable stress σ_a of the material. In addition, only the bending deformations due to the rotations of flexure hinges are taken into account to derive the maximum stress, since the axial tensile or compressive stress of the flexure hinge is far less than the maximum bending stress. Thus, we have

$$\max\{\sigma_r\} \le \sigma_a = \sigma_y/n_a, \tag{5}$$

where $n_a > 1$ is an assigned safety factor, and σ_y denotes the yield strength of the material.

For a flexure hinge bearing a bending moment around its rotation axis, the maximum angular displacement $\theta^{\max}$ occurs when the maximum stress $\sigma^{\max}$, which occurs at the outermost surface of the thinnest portion of the hinge, reaches to the yield stress σ_y.

The relationship between the maximum bending stress and maximum rotational deformation of the flexure hinge has been derived in [16]:

$$\sigma_r^{\max} = \frac{E(1+\beta)^{9/20}}{\beta^2 f(\beta)} \theta^{\max}, \tag{6}$$

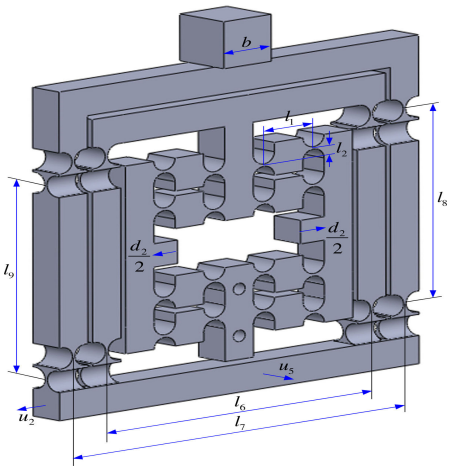

Fig. 4. Parameters of the limb #2.

where $\beta = t/2r$ is a dimensionless geometry factor, and $f(\beta)$ is a dimensionless compliance factor defined as:

$$f(\beta) = \frac{1}{2\beta + \beta^2}\left[\frac{3 + 4\beta + 2\beta^2}{(1+\beta)(2\beta+\beta^2)} + \frac{6(1+\beta)}{(2\beta+\beta^2)^{3/2}} \tan^{-1}\left(\frac{2+\beta}{\beta}\right)^{1/2}\right]. \tag{7}$$

Assume the maximum input displacement Q is applied on the input end of the amplifier in limb 1 of the XY stage, which results in a linear deflection $d_x^{\max} = A_sQ$ of the platform along the x-axis direction due to the maximum rotational deformation $\theta^{\max}$ of the hinges. According to the geometry of the stage, the maximum angular deflection may occur on the hinge belong to either the amplifier in limb #1 or the compound parallelogram flexures in limbs #2 or #3.

The maximum rotation angles occurring at the three limbs can be derived as follows:

$$\theta_1^{\max} = \frac{A_sQ/2}{\sqrt{l_1^2 + l_2^2}}, \quad \theta_2^{\max} = \frac{A_sQ/2}{l_8}, \quad \theta_3^{\max} = \frac{A_sQ/2}{l_9}, \tag{8}$$

Substituting the maximum rotation angles described by (8) into (6) allows the derivation of the relationships:

$$\sqrt{l_1^2 + l_2^2} \ge \frac{E(1+\beta)^{9/20} n_a A_s Q}{2\beta^2 f(\beta)\sigma_y}, \tag{9a}$$

$$l_8 \ge \frac{E(1+\beta)^{9/20} n_a A_s Q}{2\beta^2 f(\beta)\sigma_y}, \tag{9b}$$

$$l_9 \ge \frac{E(1+\beta)^{9/20} n_a A_s Q}{2\beta^2 f(\beta)\sigma_y}, \tag{9c}$$

which provide a guideline for the design of the stage dimension without the risk of inelastic deformations.

C. Dynamics Modeling

Resonant frequency of the XYZ stage is analytically calculated in this subsection. In order to fully describe the free vibrations of the XYZ stage, the independence of the three secondary stages should be considered as well. Thus,

TABLE I

ARCHITECTURE PARAMETERS OF AN XYZ STAGE (UNITS: MM)

r	t	h	w	l_0	l_1	l_2	l_3
2.25	0.3	6	6	6	10.5	2.2	8
l_4	l_5	l_6	l_7	l_8	l_9	b	
18	9.5	56	70	57.5	57.5	10	

TABLE II

KINEMATIC AND DYNAMIC PERFORMANCES OF AN XYZ STAGE

Performance	Amplification ratio	Input stiffness (N/μm)	Resonant frequency (Hz)
Modeling	4.74	0.865	62.29
FEA	3.79	0.868	49.59
Deviation (%)	25.1	0.35	25.6

nine generalized coordinates are selected as follows for the dynamic modeling purpose:

$$\mathbf{q} = [d_1 \quad d_2 \quad d_3 \quad u_1 \quad u_2 \quad u_3 \quad u_4 \quad u_5 \quad u_6]^T, \tag{10}$$

where d_i denotes the input displacement of the i-th motor, u_1—u_3 and u_4—u_6 describe two types of translations of the three secondary stages. The parameters of the limb #2 are depicted in Fig. 4.

The kinetic (T) and potential (V) energies for the entire stage can be expressed by the generalized coordinates only. Afterwards, substituting the kinetic and potential energies into the Lagrange's equation:

$$\frac{d}{dt} \cdot \frac{\partial T}{\partial \dot{q}_i} - \frac{\partial T}{\partial q_i} + \frac{\partial V}{\partial q_i} = F_i, \tag{11}$$

with F_i denoting the i-th actuation force, allows the generation of dynamic equation describing a free motion of the stage:

$$\mathbf{M}\ddot{\mathbf{q}} + \mathbf{K}\mathbf{q} = \mathbf{0}, \tag{12}$$

where the expressions for the 9×9 mass and stiffness matrices are omitted here for brevity.

Based on the theory of vibrations, the modal equation can be derived as:

$$(\mathbf{K} - \omega_j^2 \mathbf{M})\mathbf{\Phi}_j = \mathbf{0}, \tag{13}$$

where the eigenvector $\mathbf{\Phi}_j$ (for $j = 1, 2, \ldots, 9$) represents a modal shape and eigenvalue ω_j^2 describes the corresponding natural cyclic frequency, they can be obtained by solving the characteristic equation:

$$|\mathbf{K} - \omega_j^2 \mathbf{M}| = \mathbf{0}. \tag{14}$$

Then, the natural frequency can be computed as $f_j = \frac{1}{2\pi}\omega_j$. The lowest one among the nine natural frequencies is taken as the resonant frequency of the mechanism.

IV. MODEL VALIDATION WITH FEA

The established analytical models for the calculation of amplification ratio, input stiffness, and resonant frequency of the XYZ stage are verified by the FEA with ANSYS software package. The material is assigned as the alloy Al 7075 with the key parameters: Young's modulus = 71.7 GPa, yield strength = 503 MPa, Poisson's ratio = 0.33, and density = 2.81×10^3 kg·m^{-3}. Additionally, the architecture parameters of the stage are described in Table I, where all the hinges are designed as the identical dimension.

A. Model Validation with FEA

When a force (13 N) is applied at the two input ends of amplifier #2, a static structural analysis is carried out with FEA. The corresponding input (15 μm) and output (56.84 μm) displacements of the output platform are obtained to determine the input stiffness and amplification ratio of the stage as elaborated in Table II. Taking the FEA results as "true" values, it can be observed that analytical model overestimates the amplification ratio and input stiffness about 25.1% and 0.35%, respectively.

Besides, it is observed that the parasitic motions of the output platform along the x- and z-axes are 0.061 μm and 0.101 μm, respectively. Caused by the input motion in amplifier #2, these parasitic motions are all negligible since they only accounts for 0.11% and 0.18% of output motion of the stage, respectively. On the other hand, the induced maximum transverse motions at the input ends of amplifiers #1 and #3 are 0.047 μm and 0.033 μm, which solely equal to 0.31% and 0.22% of the input displacement, respectively. Therefore, the FEA results confirm both the input and output well-decoupling properties of the XYZ stage. Additionally, the resonant frequency is obtained by conducting a modal analysis under ANSYS environment, which shows that the first natural frequency occurs at 49.59 Hz. Whereas the analytical model overestimates the resonant frequency of the stage around 25.6%.

Referring to the performances derived by the two approaches as compared in Table II, one can observe that the maximum deviation of the derived model from the FEA results is nearly 25% while the minimum deviation is less than 1%, which are acceptable in the early design stage. The offset mainly comes from the accuracy of the adopted equations for the compliance factors and the neglect of compliances of the links between flexure hinges since these links are assumed to be rigid in the modeling procedure. In the future works, nonlinear models of the entire stage will be established to evaluate its performances more accurately.

V. ARCHITECTURE OPTIMIZATION OF THE XYZ STAGE

Before the fabrication of the XYZ stage, it is necessary to determine its architectural parameters by taking into account its performances simultaneously. To increase the natural frequency of the stage, the output platform mass is reduced by removing unnecessary mass. The stroke of the three PZT (with the length of 50 mm) is assigned as 20 μm. In addition, the FEA results for the stage performances are taken as true values. Considering that the analytical models overestimate the stage performances with deviations around 20%, a compensation factor $\eta = 0.8$ is adopted in the optimization process to compensate for the derived models.

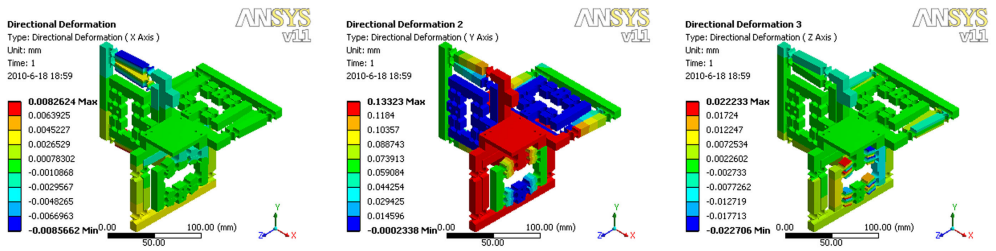

(a) (b) (c)

Fig. 5. Deformations of the XYZ stage along the (a) x-axis, (b) y-axis, and (c) z-axis with amplifier #2 driven.

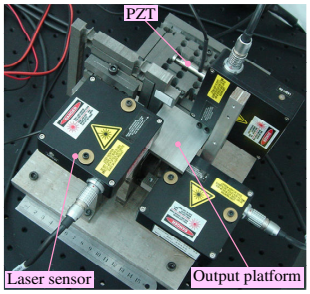

Fig. 6. The prototype XYZ stage.

A. Optimization Statement

As far as a material with a specific thickness ($w = 10$ mm in this research) is concerned, five parameters (r, t, l_1, l_2, l_8) need to be optimized since other parameters can be determined by considering the length and width restrictions of the PZT with the addition of a proper assembling space. The amplification ratio of the stage is specified to guarantee a travel range no less than 160 μm for the mobile platform. The input stiffness should not exceed the minimum stiffness of the adopted PZT, i.e., $K_{PZT} = 10\,\text{N}/\mu\text{m}$. Meanwhile, the stage should be designed with the elimination of plastic failures for the safety reason. The upper bounds for design variables are all limited so as to generate a compact manipulator. With the selection of natural frequency of the stage as an objective function, the optimization can be stated as follows:

- Maximize: Natural frequency (f)
- Variables to be optimized: r, t, l_1, l_2, and l_8
- Subject to:
  1) Amplification ratio $\eta A_s \geq 8$
  2) Input stiffness value $\eta K_a \leq K_{PZT}$
  3) Free of inelastic deflections guaranteed by (9) with a safety factor $n_a = 1.5$
  4) Parameter ranges: $3\,\text{mm} \leq r \leq 5\,\text{mm}$, $0.3\,\text{mm} \leq t \leq 2\,\text{mm}$, $2\,\text{mm} \leq l_1 \leq 20\,\text{mm}$, $1\,\text{mm} \leq l_2 \leq 4\,\text{mm}$, and $55\,\text{mm} \leq l_8 \leq 100\,\text{mm}$

B. PSO Optimization and Results

The particle swarm optimization (PSO) is adopted in the current problem due to its superiority of performance over other methods such as direct search approach and genetic algorithm (GA) [17], [18]. The optimization is implemented with MATLAB via a PSO toolbox [19], and the optimized dimensions are: r =3.00 mm, t =0.55 mm, l_1 =15.00 mm, l_2 =1.47 mm, and l_8 =55.00 mm, which leads to an XY stage with $A_s = 9.4$, $K_{in} = 11.8\,\text{N}/\mu\text{m}$, and resonant frequency $f = 124.5$ Hz, respectively.

C. Performance Test with FEA

To reveal the performances of the optimized XYZ stage, FEA simulations are carried out as well. In static FEA, with an input displacement of 20 μm applied on the input ends of the amplifier #2, the three-axis deformations of the stage are depicted in Fig. 5. It is derived that the y-axis output displacement is 131.5 μm, and the corresponding input force is 264.0 N. Thus, the optimized stage has an amplification ratio of 6.58 with an input stiffness of 13.2 N/μm. Considering that the input stiffness of the employed PZT actually lies within 14–208 N/μm, the actuator can work properly for the drives of the stage. Besides, the maximum stress generated by FEA is 64.8 MPa, which is far less than the yield stress (503 MPa) of the material. In addition, it is observed that the parasitic motions along the x- and z-axes are negligible.

Moreover, the modal analysis results demonstrate that the resonant frequency of the XYZ stage is 78.7 Hz. It is known that the resonance frequency of the stage structure can be magnified by increasing the stiffness or reducing the equivalent mass of the stage. For instance, the material with a thinner thickness can be used for fabrication and unnecessary mass of the moving parts can be removed to achieve a resonance frequency higher than 100 Hz. In the following discussions, a prototype of the XY stage is developed for performance test.

VI. PROTOTYPE FABRICATION AND TESTING

A. Prototype Fabrication

A prototype XYZ stage is developed as shown in Fig. 6. The three limbs of the stage are fabricated by the wire EDM process from alloy Al 7075. Concerning the actuation, three 20 μm-stroke PZTs (model PAS020 produced by Thorlabs, Inc.) are adopted to drive the XYZ stage. A PCI-based D/A board (PCI-6703 with 16-bit D/A converters from National Instruments Corp.) is employed to produce an analog voltage, which is then amplified by a piezo-amplifier (BPC002 from the Thorlabs) to provide a voltage of 0–75 V for the drives of the PZTs. In order to measure the output displacements of the moving platform, three laser displacement sensors (Microtrak II, head model: LTC-025-02, measuring range: 2.5 mm, from MTI Instruments, Inc.) are used. The analog voltage outputs of the three sensors are read simultaneously by a PC through a peripheral component interconnect (PCI)-based data acquisition (DAQ) board (PCI-6034E with 16-bit A/D converters, from the National Instruments). It can be calculated that the resolution of the position detection system is 0.038 μm.

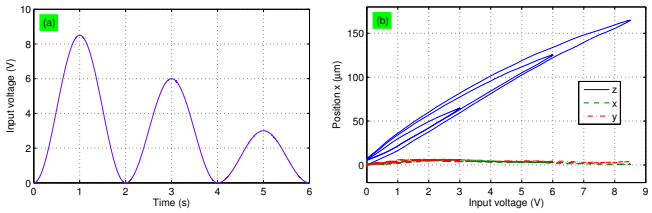

Fig. 7. (a) Input voltage signal applied to the PZT #3; (b) output motions of the XYZ stage in the three axes.

B. Experimental Testing and Results

The open-loop static properties of the XY stage are experimentally tested. With a 0.5-Hz sinusoidal voltage signal ranging from 0 to 8.5 V [see Fig. 7(a)] provided by the D/A board, which is then applied to the piezo-amplifier to produce a voltage of 0–75 V to drive the PZT #3, the three axial translations of the XYZ stage are all recorded in Fig. 7(b). As expected, with the open-loop voltage-driven strategy, the PZT exhibits nonlinearity mainly attributed to the hysteresis effects. Specifically, the relationship between the stage output displacement and input voltage of PZT is nonlinear as illustrated by hysteresis loops in Fig. 7(b). It is observed that the maximum translational motions in the z-, x- and y-axes are 164.8 μm, 6.7 μm, and 7.2 μm, respectively.

In view of the stroke (20 μm) of the PZT, the amplification ratio of the stage can be determined as 8.2, which is larger than the FEA result. The reason mainly comes from the preloading effect of the PZT mounting. Since the PZT is inserted into the mechanical amplifier and preloaded using a screw, the initial values for the parameters l_x and l_y (see Fig. 4) are increased and deceased, respectively. Hence, the ratio of l_x/l_y is greater than the nominal value. Thus, an amplification ratio larger than the expected value is achieved.

Moreover, comparing to the predominant z-axis motion, the parasitic translations in the x- and y-axes account for 4.1% and 4.4%, respectively. The experimental results demonstrate the low-level parasitic motions of the XYZ stage, which allows the employment of SISO controller designs for the three axes in the future works. The crosstalk between the three axes mainly comes from manufacturing errors of the stage, mounting errors of the displacement sensors with respect to sensor targets, and Abbe errors due to the offset distance between the measurement point and motion axis direction of the stage. The piezoelectric hysteresis effects and cross-axis errors will be compensated by a closed-loop controller design in the next step research. The positioning repeatability and accuracy will be calibrated as well.

VII. CONCLUSION

The design, modeling, simulation, and experimental testing of a new decoupled XYZ parallel micropositioning stage are reported in this paper. The stage owns a simple structure and has both input and output decoupling properties in virtue of motor isolation and decoupled output motion. A displacement amplifier with large transverse stiffness is adopted to amplify the linear motor's stroke and to isolate the motors. Based on the derived analytical models of the stage, dimension optimization is performed to achieve an XYZ stage with maximal natural frequency subject to the workspace and stiffness performance constraints. With the optimized parameters, a prototype XYZ stage is fabricated and its kinematics performances are tested. Experimental results show that the crosstalk between the working axes is less than 4.5%, which indicates a nice decoupling property of the developed XYZ stage. In our future works, the piezoelectric nonlinearity of the stage will be suppressed by a suitable control system design, and the application in manipulating microscopic objects will be performed to demonstrate the stage ability as well.

REFERENCES

[1] J. Hesselbach and A. Raatz, "Pseudo-elastic flexure-hinges in robots for micro assembly," in *Proc. of SPIE*, vol. 4194, 2000, pp. 157–167.
[2] B.-J. Yi, G. Chung, H. Na, W. Kim, and I. Suh, "Design and experiment of a 3-DOF parallel micromechanism utilizing flexure hinges," *IEEE Trans. Robot. Automat.*, vol. 19, no. 4, pp. 604–612, 2003.
[3] S. Awtar and A. H. Slocum, "Constraint-based design of parallel kinematic XY flexure mechanisms," *ASME J. Mech. Des.*, vol. 129, no. 8, pp. 816–830, 2007.
[4] J.-C. Shen, W.-Y. Jywe, H.-K. Chiang, and Y.-L. Shu, "Precision tracking control of a piezoelectric-actuated system," *Precis. Eng.*, vol. 32, no. 2, pp. 71–78, 2008.
[5] R.-F. Fung, Y.-L. Hsu, and M.-S. Huang, "System identification of a dual-stage XY precision positioning table," *Precis. Eng.*, vol. 33, no. 1, pp. 71–80, 2009.
[6] www.physikinstrumente.com/en/products/prdetail.php?sortnr=800900.
[7] J. E. McInroy, "Modeling and design of flexure jointed stewart platforms forcontrol purposes," *IEEE/ASME Trans. Mechatron.*, vol. 7, no. 1, pp. 95–99, 2002.
[8] X.-J. Liu, J. I. Jeong, and J. Kim, "A three translational DoFs parallel cube-manipulator," *Robotica*, vol. 21, no. 6, pp. 645–653, 2003.
[9] T.-F. Niaritsiry, N. Fazenda, and R. Clavel, "Study of the sources of inaccuracy of a 3 DOF flexure hinge-based parallel manipulator," in *Proc. of IEEE Int. Conf. on Robotics and Automation*, 2004, pp. 4091–4096.
[10] H.-H. Pham and I.-M. Chen, "Stiffness modeling of flexure parallel mechanism," *Precis. Eng.*, vol. 29, no. 4, pp. 467–478, 2005.
[11] K. A. Jensen, C. P. Lusk, and L. L. Howell, "An XYZ micromanipulator with three translational degrees of freedom," *Robotica*, vol. 24, no. 3, pp. 305–314, 2006.
[12] H. Wang and X. Zhang, "Input conpuling analysis and optimal design of a 3-DOF compliant micro-positioning stage," *Mech. Mach. Theory*, vol. 43, no. 4, pp. 400–410, 2008.
[13] Y. Li and Q. Xu, "Design and analysis of a totally decoupled flexure-based XY parallel micromanipulator," *IEEE Trans. Robot.*, vol. 25, no. 3, pp. 645–657, 2009.
[14] X. Tang and I.-M. Chen, "A large-displacement 3-DOF flexure parallel mechanism with decoupled kinematics structure," in *Proc. of IEEE Int. Conf. on Intelligent Robots and Systems*, 2006, pp. 1668–1673.
[15] Y. Amirata, F. Artiguea, and J. Pontnau, "Six degrees of freedom parallel robots with C5 links," *Robotica*, vol. 10, no. 1, pp. 35–44, 1992.
[16] S. T. Smith, *Flexures: Elements of Elastic Mechanisms*. New York: Gordon and Breach, 2000.
[17] M. Clerc and J. Kennedy, "The particle swarm-explosion, stability, and convergence in a multidimensional complex space," *IEEE Trans. Evol. Comput.*, vol. 6, no. 1, pp. 58–73, 2002.
[18] Q. Xu and Y. Li, "Error analysis and optimal design of a class of translational parallel kinematic machine using particle swarm optimization," *Robotica*, vol. 27, no. 1, pp. 67–78, 2009.
[19] B. Birge, "PSOt – a particle swarm optimization toolbox for use with Matlab," in *Proc. of IEEE Swarm Intelligence Symposium*, Indianapolis, Indiana, USA, 2003, pp. 182–186.